Computational Materials Science 182 (2020) 109749

Contents lists available at ScienceDirect

Computational Materials Science

journal homepage: www.elsevier.com/locate/commatsci

Solidification and heat treatment simulation for aluminum alloys with scandium addition through CALPHAD approach

Rajesh Jha[a,b,*], George S. Dulikravich[a]

[a] MAIDROC Laboratory, Mechanical and Materials Engineering Department, Florida International University, Miami, FL 33174, USA
[b] Department of Mechanical Engineering, Colorado School of Mines, Golden, CO 80401, USA

ARTICLE INFO

Keywords:
Aluminum alloys
CALPHAD
Deep Learning Artificial Neural Network (DLANN)
Scheil-Gulliver's solidification simulation
Heat treatment
Interfacial energy

ABSTRACT

Scandium, and scandium combined with zirconium, improves multiple properties of aluminum based alloys. In this work, we performed solidification and heat treatment simulations for studying precipitation kinetics of Al_3Sc crystals within the framework of CALPHAD approach on novel candidate alloy compositions from our previous work belonging to 2XXX, 6XXX and 7XXX class of aluminum alloys. In our previous work, computational study was performed on stability of various stable and metastable phases along with thermodynamically stable Al_3Sc phase in heat-treatable aluminum alloys of 2XXX, 6XXX and 7XXX series by application of several concepts of artificial intelligence on phase stability data generated under the framework of CALPHAD approach. We considered 12 elements for 2XXX, 10 elements for 6XXX and 11 elements for 7XXX class of alloys, thus selected a comparatively large multicomponent system when compared to works reported on aluminum alloys through CALPHAD approach. In 2XXX and 7XXX series, both Sc and Zr were included, while in 6XXX series only Sc was added. Software Thermocalc was used to generate phase stability data. For proper precipitation of Al_3Sc crystals during heat treatment, it is important that Al_3Sc is present in the melt. Hence, solidification simulation (Scheil–Gulliver) was performed, followed by heat treatment simulation at various temperatures for a few candidate alloys belonging to these three series of aluminum alloys with Sc added. Additional strengthening phases were also considered in aluminum base alloys of these three series in our previous work. The presented computational approach can be useful and can be used as a screening tool for selecting a chemical composition and heat treatment protocol prior to performing experiments.

1. Introduction

In structural materials, aluminum alloys are preferred over other alloys due to superior strength to weight ratio. Strength in these alloys is achieved by ageing or precipitation hardening [1,2]. Precipitation hardening phases depend on the major alloying element and its composition [1,3]. Aluminum alloys have been divided into several classes based on the major alloying element in addition to aluminum [4].

One of the problems with aluminum alloys is their poor corrosion resistance [1]. In recent years, a significant amount of research has been reported on the use of scandium in aluminum alloys [1] with the objective of improving the anti-corrosion potential of aluminum alloys even when scandium is added in small amounts [1]. Regarding precipitation hardening, research shows that scandium is one of the best alloying elements that enhances strengthening mechanism by precipitation hardening in aluminum alloys, where some reports also suggest that only gold is better than scandium in enhancing strengthening of these alloys [1]. One of the factors that limit precipitation of Al_3Sc phase is the temperature regime of precipitation of Al_3Sc during heat treatment [1–3,5,6]. Al_3Sc precipitates at about 300 °C, while other phases that strengthen aluminum alloys precipitate around 160–200 °C [1–3,5,6]. In non-heat-treatable alloys, strengthening by Al_3Sc plays an important role [1]. In heat-treatable alloys, it is important that some amount of Al_3Sc is present in the melt to enhance the precipitation of Al_3Sc phase in the desired grain size range as a limited amount of Sc can be precipitated from supersaturated solution [1,2].

First phase diagrams of the Al-Sc system appeared in the USSR in 1964 [1]. In these diagrams, four phases were shown, Al_3Sc, Al_2Sc, AlSc and $AlSc_2$, where Al_3Sc is an equilibrium phase, or is the phase which is in thermodynamic equilibrium with Al [1]. Since the 1980's, aluminum alloys containing Sc have been systematically developed and some parts of military aircraft have been manufactured from Al-Li alloys

* Corresponding author at: Postdoctoral Researcher, MAIDROC Laboratory, Mechanical and Materials Engineering Department, Florida International University, Miami, Florida 33174, USA.
E-mail addresses: rjha001@fiu.edu, rjha@fiu.edu (R. Jha).

https://doi.org/10.1016/j.commatsci.2020.109749
Received 25 December 2019; Received in revised form 8 April 2020; Accepted 14 April 2020
Available online 26 April 2020

containing Sc [1]. In the USA, application of aluminum alloys containing Sc started in 1997, when Easton introduced baseball bats manufactured from 7XXX series Al base alloy containing Sc that was developed by Ashurst Technology and Kaiser Aluminum. AlCoA soon followed the trend and introduced a new Louisville Slugger series of baseball bats. Easton later launched light-weight tubing for bicycle frames using Sc-containing 7xxx series aluminum alloy [1]. Gun manufacturer Smith and Wesson introduced a series of handguns where the frame was made from aluminum alloys containing Sc [1]. One of the challenges of using Sc in commercial alloys in large scale is the availability of Sc and cost of the master alloy that is used in alloying. Even an addition of 0.2 wt% Sc can significantly increase the price of the final alloy. Based on the size of the product, this price increase can be 3–4 times the cost of the base aluminum alloys, which is difficult to sustain financially [1].

Commercial software based on CALPHAD approach like Thermocalc [7,8] provides the user with thermodynamic database TCAL5 [9] and mobility database MOBAL4 [10], which contains elements used in commercial aluminum alloys [11] along with scandium [9,10]. Aluminum alloys as well as the scandium addition in aluminum alloys have been studied within the framework of CALPHAD approach [11–19]. Current state of the art focuses on understanding the stability of metastable phases [3] responsible for targeted properties as well as heat treatment [11–19]. One of the limitations of the current state of art is that most of the research is focused on compositions around known alloys and conclusions are drawn on the basis of slight deviation in the composition of the known alloys or a small amount of addition of a new element on a known composition [11–19]. Another limitation is that most of the reported work focuses on studying aluminum alloys with maximum 6–8 elements [2–6,11–19].

We formulated our research problem to address these limitations that is to move away from known compositions as well as considered 10–12 alloying elements (similar to commercial alloys). We divided our work in two parts. In our previous work [20], we performed a computational study of the phase stability of precipitation strengthening phases in 2XXX, 6XXX and 7XXX series aluminum base alloys that include scandium. Thereafter, we used the phase stability data to develop Deep-Learning Artificial Neural Network (DL-ANN) models. We wrote our code in the Python programming language using Tensorflow [21] and Keras [22] libraries. DL-ANN models were used to determine the amount of metastable phase in the presence of stable phases for a given composition and temperature. Thereafter, we analyzed thousands of compositions to draw various correlations as well as select a few candidates, which will provide with the optimum amount of stable and metastable phases for further study.

In this work, we selected a few candidates from our previous work [20] for studying the precipitation kinetics of Al_3Sc phase in aluminum alloys (2XXX, 6XXX and 7XXX). These candidates are novel and not reported before and were chosen after thorough investigation through CALPHAD and Artificial Intelligence. Computational simulation under the framework of CALPHAD approach was performed in two stages. Initially we performed Scheil-Gulliver's solidification simulation for determining the formation of Al_3Sc phase from the melt. Thereafter, heat treatment simulation was performed to study the precipitation kinetics (nucleation, growth and coarsening) of Al_3Sc phase in these classes of alloys. Computation time varied a lot and depended on the number of elements considered in an alloy. On an average, for 10 elements (6XXX) it took about 3–4 h and for 12 elements (2XXX) it was about 7–8 h, while for 11 elements (7XXX) it took about 4–5 h. During simulation, sometimes the system freezes or crashes. In order to avoid that, we tried to run one simulation at a time. That is, we simulated heat treatment at 4 different temperatures. Executing all four cases at the same time led to crashing particularly in 2XXX with 12 elements. We have reported the computational infrastructure used in Materials and Methods section. Thus, a user can use Deep-Learning Artificial Neural Network (DL-ANN) models from our previous work to ascertain equilibrium amount of phases for any new composition, even on a cell phone in a few seconds prior to performing heat treatment simulation through CALPHAD approach or performing experiments for avoiding wastage of time and resources. Deep-Learning Artificial Neural Network (DL-ANN) models can be used for free and we have tested it on an Android phone with 6 GB RAM which costs about $200.

Our research team has expertise in application of several concepts of artificial intelligence on data generated through CALPHAD approach as well as experiments when designing titanium alloys [23], nickel-base superalloys [24], hard magnets (AlNiCo) [25] and soft magnets (FINEMET) [26–29], where simulation results were experimentally verified and analyzed by advanced diagnostic tools. Thus, we framed our problem in a way that we can provide researchers with a predictive tool based on CALPHAD approach and Artificial Intelligence (Deep learning) which can be used for screening aluminum alloys prior to performing experiments.

2. Materials and methods

In this study, three classes of aluminum based alloys were chosen. These classes of alloys are heat treatable. Each of these classes consists of several alloying elements. Initial classification was based on particular alloying elements [4] as follows. 2XXX for alloys with Cu, 6XXX alloys with Mg and Si, and 7XXX alloys with Zn.

For each class of these alloys, bounds for concentrations for each of the alloying elements were specified based on data available in the literature [1]. Variable bounds for chemical composition of alloy series 2XXX, 6XXX and 7XXX has been tabulated in Table 1. It should be pointed out that for series 2XXX and series 7XXX, Sc and Zr were both added, while for series 6XXX only Sc was added.

Using commercial software, Thermocalc 2018B [7], calculations were performed to study how to stabilize the metastable phases in 2XXX, 6XXX and 7XXX aluminum based alloys with scandium additions as discussed in our previous work [20]. In this work, we used the findings from our previous work [20] to perform solidification simulations based on Scheil-Gulliver theory to study the formation of fully Al_3Sc phase from Al3X. It was followed by heat treatment simulations in order to study the precipitation kinetics or nucleation, growth and coarsening of Al_3Sc phase. Thermodynamic database TCAL5 [9] and mobility database MOBAL4 [10] were used for performing equilibrium calculations and studying kinetics of precipitation of Al_3Sc phase. Al_3Sc is a stable phase and can be estimated from equilibrium calculations [3]. In Thermocalc database, it exists as Al3X phase [3,7,8]. In the presence of Zr, Al3X can be $Al_3(Sc_xZr_{1-x})$ [3,5,6]. This will be mentioned in the heat treatment section in detail.

Phase transformations in these three series of aluminum based alloys are as follows.

Table 1
Bounds on concentrations of alloying elements (wt.%) for three series of alloys.

	2XXX series		6XXX series		7XXX series	
Element	min.	max.	min.	max.	min.	max.
Si	0.20	1.20	0.20	1.80	0.12	0.50
Fe	0.30	0.50	0.10	0.70	0.15	0.50
Cu	3.80	6.80	0.10	0.40	0.10	2.40
Mn	0.20	1.20	0.05	1.10	0.05	0.70
Mg	0.02	1.80	0.35	1.40	0.80	3.70
Cr	0.00	0.10	0.00	0.35	0.00	0.30
Zn	0.10	0.25	0.05	0.25	3.80	8.30
Ti	0.02	0.15	0.00	0.20	0.01	0.20
V	0.00	0.15	0.00	0.00	0.00	0.00
Zr	0.00	0.25	0.00	0.00	0.00	0.20
Sc	0.00	10.00	0.00	10.00	0.00	10.00
Al	Balance to 100.00		Balance to 100.00		Balance to 100.00	

- 2XXX series: For alloys containing Cu, precipitation hardening phases are θ (Al_2Cu) which transforms to θ' and it transforms into θ'' which transforms into GP (Guinier–Preston) zones. The objective should be to suppress θ (Al_2Cu) from equilibrium calculations to stabilize θ' and suppress θ (Al2Cu) and θ' in order to stabilize θ''. Here, θ' is the major strengthening phase [1,3].
- 6XXX series: In the presence of Mg, β (Mg_2Si) is the stable phase and the metastable phases are β', β'' and GP zones. Here, β' is the major strengthening phase [1,3].
- 7XXX series: For Zn containing alloy, the phases are η, η' and GP zones [1].

Phase stability in these three series of aluminum based alloys can be studied as follows:

- In our previous work [20], a significant amount of data was generated for stable and metastable phases for 2XXX, 6XXX and 7XXX series so that response surfaces can be generated for these phases. Deep Learning Artificial Neural Network (DLANN) was developed using TensorFlow/Keras libraries in Python language and used in this research.
- For each of the three series of Al-based alloys, one alloy was chosen from the computational analysis through Self Organizing Maps (SOM) for simulating nucleation and growth of Al_3Sc phase at various annealing temperatures.

For precipitation of Al_3Sc during annealing, it is important to ensure that there is Al_3Sc phase present in the melt during solidification. Al_3Sc phase is precipitated during heat treatment/ annealing at around 300 °C [1]. For targeted properties, the desired grain size range is about 2–6 nm [1]. Apart from solidification and heat-treatment, Al_3Sc can be precipitated by hot working/ deformation at around 400–600 °C [1]. As already mentioned, Al_3Sc is a stable phase and can be estimated from equilibrium calculations [1,3]. In Thermocalc database, it exists as Al3X phase [3,8]. In the presence of Zr, Al3X can be $Al_3(Sc_xZr_{1-x})$ [3,8]. From Scheil–Gulliver simulations, it is possible to estimate the temperature at which the fully Al_3Sc phase is obtained and the amount of Al_3Sc phase precipitated during solidification [2,7]. Thereafter, simulations of annealing were performed at 300, 350, 400 and 450 °C for each of the cases for 1000 h. Interfacial energy had to be optimized in order to obtain desired grain size that can be verified from the literature. In this case, the nucleation sites were in the bulk.

Scheil–Gulliver simulations: were performed in Thermocalc [7] to determine solidification path or sequence of appearance of various phases from the melt under thermodynamic equilibrium conditions [2,14]. In our work, we focused on Al_3Sc phase and its precipitation in the melt. In this model, it is assumed that liquid phase is chemically homogeneous throughout the process. Therefore, diffusion in liquid is extremely fast, whereas there is no diffusion within the solid phases. This leads to formation of concentration gradients inside the solid phases and leads to microsegregation [2].

Kampmann-Wagner Numerical (KWN) approach [30,31]*:* In Thermocalc [7], precipitation module TC-PRISMA [8] is based on Langer-Schwartz theory and it uses the Kampmann-Wagner Numerical (KWN) approach [30,31] to simulate simultaneously occurring phenomena of nucleation, growth, and coarsening. The Langer and Schwartz theory [7,8,32,33] is a fast-acting model used for simulation of particle number density and mean size of the precipitated phase. The KWN method [30,31] is an extension of the Langer-Schwartz approach and its modified form [32]. KWN is also used for prediction of particle size distribution (PSD) over the full course of precipitation [8,32]. Furthermore, this module can analyze the size distribution of precipitates over the complete thermal treatment protocol applied to multi-component systems and multiphase alloys [32].

For the modeling, we considered the FCC_L12 phase as FCC matrix and AL3X as Al_3Sc precipitate from Thermodynamic database TCAL5 [9] and mobility database MOBAL4 [10]. Molar volume of AL3X phase was taken from the database, while a user can change it. Initial number of nucleation sites (N_0) were calculated from the matrix setting by Thermocalc [8] and it depends on molar volume of matrix phase. The nucleation sites were set to occur in the bulk (in TC-PRISMA, a user can set nucleation sites in bulk, at grain boundaries, or at dislocations). Dislocation density was kept at a constant value of $6.0*10^{12}\ m^{-2}$. Grain aspect ratio was kept at a constant value of 1.0. Mobility enhancement prefactor was set by trial and error at 5.

From classical nucleation theory [34], time dependent nucleation rate J_t can be expressed as

$$J_t = J_s \exp\left(\frac{-\tau}{t}\right) \tag{1}$$

In equation (1), J_s is the steady state nucleation rate, τ is the incubation time for establishing steady state nucleation conditions, and t is the isothermal incubation time.

Steady state nucleation rate J_s can further be expressed as [34]

$$J_s = Z\beta^* N_0 \exp\left(\frac{-\Delta G^*}{kT}\right) \tag{2}$$

Thus, number density N_t can be written as

$$N_t = \int J_t dt \tag{3}$$

In equation (2), Z is the Zeldovich factor, β^* is attachment rate of solute atoms to Al_3Sc crystals, N_0 is the number of available nucleation sites, ΔG^* is the Gibbs energy or activation energy of forming Al_3Sc crystals, k is the Boltzmann's constant, and T is absolute temperature. As mentioned above, N_0 was calculated from the matrix settings.

Isothermal incubation time, τ can be expressed as shown in equation (4). In Thermocalc [8], $\theta = 2$ is adopted, though value of θ can vary from one derivation to another [8,30,34,35].

$$\tau = \frac{1}{\theta Z^2 \beta^*} \tag{4}$$

Equation (5) describes the initial number density as a function of Gibbs energy.

$$N_0 \exp\left(\frac{-\Delta G^*}{kT}\right) \tag{5}$$

Gibbs energy or activation energy of forming Al_3Sc crystals, ΔG^* can be expressed as:

$$\Delta G^* = \frac{16\pi}{3} \frac{\sigma_{int}^3}{\left(\frac{\Delta G_m^{FCC-Al_3Sc}}{V_m^{Al_3Sc}}\right)^2} \tag{6}$$

In equation (6), $\Delta G_m^{FCC-Al_3Sc}$ is the molar Gibbs energy of formation of Al_3Sc nanocrystals from the FCC matrix and $V_m^{Al_3Sc}$ is the molar volume of Al_3Sc nanocrystals [31]. σ is the interfacial energy between the FCC matrix phase and precipitate Al_3Sc phase.

Zeldovich factor (Z), and attachment rate of solute to Al_3Sc crystals (β^*) can be expressed as shown by equation (7) and (8) respectively [18,36,37].

$$Z = \frac{V_m^{Al_3Sc}}{2\pi N_A R^{*2}} \sqrt{\frac{\sigma}{kT}} \tag{7}$$

$$\beta^* = \frac{2\pi R^{*2}}{(l^{Al_3Sc})^4} \left[\sum \frac{(\bar{X}_i^{Al_3Sc} - \bar{X}_i^{FCC})^2}{\bar{X}_i^{FCC} D_i^{FCC}} \right]^{-1} \tag{8}$$

In equation (8), $\bar{X}_i^{FCC}$ is the equilibrium composition of element i in the FCC phase while $\bar{X}_i^{Al_3Sc}$ is the equilibrium composition of element i in the Al_3Sc phase. D_i^{FCC} is the chemical diffusion coefficient of element i in the FCC phase, which is calculated by Thermocalc [7] using thermodynamic database, TCAL5 [9], and the mobility database, MOBAL4

[10].

Critical radius (R^*) can be calculated as shown in equation (9) [30,31].

$$R^* = -\frac{2\sigma V_m^{Al_3Sc}}{\Delta G_m^{FCC-Al_3Sc}} \tag{9}$$

Al_3Sc nanocrystals will grow continuously due to supersaturation of the FCC matrix phase and its radius $R_t^{Al_3Sc}$ can be modeled as shown in equation (10) [38,39]

$$\frac{dR_t^{Al_3Sc}}{dt} = \frac{D_i^{FCC}}{\xi_{i,t} R_t^{Al_3Sc}} \frac{X_{i,t}^{FCC} - \bar{X}_i^{FCC}}{\bar{X}_i^{Al_3Sc} - \bar{X}_i^{FCC}} \tag{10}$$

In equation (10), $\bar{X}_i^{Al_3Sc}$ is the equilibrium composition of Al_3Sc phase while $X_{i,t}^{FCC}$ is the composition of supersaturated FCC matrix phase. Growth of Al_3Sc crystals is dependent on the composition of remaining FCC matrix phase $X_{i,t}^{FCC}$. Thus, mass balance equation will be as follows [37]

$$X_{i,t}^{FCC} = (X_{i,0}^{FCC} - V_f^{Al_3Sc} \bar{X}_i^{Al_3Sc})/(1 - V_f^{Al_3Sc}) \tag{11}$$

The expression $\xi_{i,t} R_t^{Al_3Sc}$ is the effective diffusion distance from FCC matrix and Al_3Sc interface and is estimated using mass balance equation shown in equation (11) and by mean field approximation based on volume fraction of Al_3Sc crystals. The parameter $\xi_{i,t}$ by solving equation (12) [37–39]

$$\xi_{i,t} = 1 - \lambda_{i,t}\pi \exp(\lambda_{i,t}^2)\mathrm{erfc}(\lambda_{i,t}) = \frac{1}{2\lambda_{i,t}^2} \frac{X_{i,t}^{FCC} - \bar{X}_i^{FCC}}{\bar{X}_i^{Al_3Sc} - \bar{X}_i^{FCC}} \tag{12}$$

In equation (12), $\lambda_{i,t}$ is a numerical parameter that can be calculated by solving equation (13) [38–40].

$$2\lambda_{i,t}^2 - 2\lambda_{i,t}^3 \sqrt{\pi} exp(\lambda_{i,t}^2) erfc(\lambda_{i,t}) = \frac{X_{i,t}^{FCC} - \bar{X}_i^{FCC}}{\bar{X}_i^{Al_3Sc} - \bar{X}_i^{FCC}} \tag{13}$$

During isothermal annealing, growth mechanism will transform into coarsening, when the composition is fully partitioned between FCC matrix phase and Al_3Sc phase. Perez et al [39,41] proposed a way to predict coarsening rate by using growth equation and linearized form of the Gibbs-Thomson effect as shown in equation (14).

$$\frac{dR_t^{Al_3Sc}}{dt} = \frac{8}{27} \frac{\sigma V_{at}^{Al_3Sc}}{(R^{Al_3Sc})^2 kT} \frac{D_i^{FCC} \bar{X}_i^{FCC}}{\bar{X}_i^{Al_3Sc} - \bar{X}_i^{FCC}} \tag{14}$$

In equation (14), $V_{at}^{Al_3Sc}$ is the mean atomic volume of Al_3Sc phase and N_A is the Avogadro's number.

$$V_{at}^{Al_3Sc} = \frac{V_m^{Al_3Sc}}{N_A} \tag{15}$$

During the course of annealing, mean radius ($\bar{R}_t^{Al_3Sc}$) and volume fraction ($V_{f,t}^{Al_3Sc}$) of Al_3Sc nanocrystals can be calculated from the number density of Al_3Sc nanocrystals at each time step using equation (3). In other words, precipitate radius can be correlated to number density using size distribution function [36,38,39]. Mean radius at any time step can thus be calculated as shown in equation (16), while volume fraction of Al_3Sc nanocrystals can be estimated using equation (17).

$$\bar{R}_t^{Al_3Sc} = \frac{\sum N_t R_t^{Al_3Sc}}{\sum N_t} \tag{16}$$

$$V_{f,t}^{Al_3Sc} = \sum N_t \frac{4\pi (R_t^{Al_3Sc})^3}{3} \tag{17}$$

Computational infrastructure: Regarding computational infrastructure, operating system was Windows 10, i7 processor with 16 GB RAM. Thermocalc was installed in a computer lab so license was not a single user license. Computation time depends on complexity or number of alloying elements in an alloy particularly for precipitation kinetic simulation. For solidification/ Scheil-Gullivers simulation, the average time was between 5 and 10 min for the entire simulation. For precipitation kinetics we ran four simulations together, that is 4 isothermal heat treatment simulations for 1000 h annealing time. Aluminum alloy of class 2XXX contains 12 elements, thus it took about 7–8 h to run the simulation. Aluminum alloy of class 6XXX contains 10 elements, thus it took about 3–4 h to run the simulation. Aluminum alloy of class 7XXX contains 11 elements, thus it took about 4–5 h to run the simulation. During the precipitation kinetics simulation for 2XXX and 7XXX, computer froze several times and sometimes it crashed. It can be possible that there were other users on a group license that may have caused crashes of simulation as we have mentioned that Thermocalc was installed in a computer lab.

3. Results and Discussions

As stated above, we have divided this work in two parts: phase stability (equilibrium) and solidification, and heat treatment.

3.1. Phase transformation: Phase stability (equilibrium) and solidification

Based on phase stability calculation results from our previous work [20], a few compositions were selected for each of three series of Al-based alloys and solidification and heat treatment simulations were performed on them. Table 2 lists the composition (wt. %) for alloys chosen for further examination. For the chosen 2XXX series alloy, under equilibrium conditions at 300 °C, calculated equilibrium phases are shown in Table 3. Composition of alloy was chosen in a way that Sc content is less than 1 wt%.

Table 2 also lists the composition (wt. %) for 6XXX series alloy chosen for further examination. Under equilibrium conditions at 163.70344 °C, equilibrium phases are tabulated in Table 4. Alloy in this case does not contain Zr, thus, differs from 2XXX and 7XXX series of alloys. In this case, higher amount of Sc was allowed to be used.

Table 2 also lists the composition (wt. %) for 7XXX series alloy chosen for further examination. Under equilibrium conditions at 353.4942 °C, equilibrium phases are tabulated in Table 5. Composition of alloy was chosen in a way that Sc content is less than 1 wt%. Notice that 7XXX series also contains Zr.

In Table 5, it can be observed that AL3X is not entirely Al_3Sc. Hence, solidification simulations are important to determine the temperature at which the AL3X precipitate will be fully Al_3Sc. Additionally, it is possible to estimate the amount (mole fraction) of Al_3Sc as well as the liquidus temperature, that is, the temperature above which all the alloying constituents are fully molten and represent a liquid.

Table 6 shows important results obtained from the Scheil-Gulliver

Table 2
Compositions of three series of Al-based alloys chosen for heat treatment simulation.

Alloying element	2XXX series	6XXX series	7XXX series
Si	0.38828	1.5497	0.28606
Fe	0.3919	0.57313	0.21862
Cu	4.95088	0.27893	1.51113
Mn	0.32005	0.63697	0.36188
Mg	0.53321	1.07076	1.05662
Cr	0.04353	0.1437	0.12353
Zn	0.19235	0.11882	3.73898
Ti	0.04297	0.13088	0.15506
V	0.09389	0.0	0.0
Zr	0.21774	0.0	0.17829
Sc	0.92541	2.60077	0.75953
Al	91.89979	92.89525	91.61031

Table 3
Equilibrium amount (mole) of critical phases at a given temperature for 2XXX alloy.

Equilibrium (2XXX)	Temperature	AL3X	THETA_PRIME
	300 °C	0.02628	0.03594

Table 4
Equilibrium amount (mole) of critical phases at a given temperature for 6XXX alloy.

Equilibrium (6XXX)	Temperature	AL3X	BETA_PRIME
	163.70344 °C	0.04696	0.01786

simulations for each of the Al-based series of alloys that also contain Sc. Specifically, it shows the liquidus temperature of each alloy, temperature at which AL3X precipitates as fully Al_3Sc, amount of Al_3Sc precipitated after solidification, and mole fraction of the solid phase of the alloy. Among the three series of alloys studied, 6XXX series has the highest amount of Sc followed by 2XXX and 7XXX series which has the lowest amount of Sc. It should be observed that 6XXX series has the highest liquidus temperature, thus, melting point. This information can be helpful during the design of heat treatment for the aluminum alloy system.

Results from the Scheil-Gulliver simulations for 6XXX and 7XXX series alloys are shown as curves in Fig. 1 and Fig. 2, respectively. These two alloys were chosen since their temperatures at which AL3X is fully Al_3Sc are close even though 6XXX contains high amount of Sc and no Zr; while 7XXX contains the lowest amount of Sc and includes Zr.

In both Fig. 1 and Fig. 2, the legends show the sequence of precipitation of various phases during solidification. Since it is a multi-component system, there is a possibility of precipitation of several phases during solidification and various equilibriums can exist simultaneously. Scheil solidification curve is different from the phase diagram as phase diagram is plotted under equilibrium conditions. The Scheil solidification curve also shows deviation from equilibrium, as can be seen in Fig. 1, where the dotted line represents equilibrium. Additionally, Scheil solidification stops when all of liquid is completely solidified, while in phase diagram solid–solid transformations are possible [2].

3.2. Heat treatment

In order to perform heat treatment within the framework of CALPHAD approach, it is very important to use the correct interfacial energy. In this work, we calibrated our model on the basis of experimental and reported values of interfacial energy in the literature for Al_3Sc precipitation from the FCC_L12 matrix phase. For a class of Al-Mg-Sc alloys, average reported values of interfacial energy for annealing temperatures of 300, 350, 400 and 450 °C were, respectively, 135, 130, 125 and 115 mJ m^{-2} [19]. These values were used as a starting point and modified in its vicinity so as to successfully simulate the nucleation and growth of Al_3Sc crystals for the cases where a few additional alloying elements were considered.

Fig. 3 shows the nucleation and growth kinetics of Al_3Sc phase during isothermal annealing at 300, 350, 400 and 450 °C for a 2XXX series alloy containing both Sc and Zr (Sc: 0.92541 wt%; Zr: 0.21774 wt %). The annealing time was extended to 1000 h to see the effect of time on coarsening of Al_3Sc grains. Here, it can be observed that for isothermal annealing at 300 and 350 °C, mean grain size stabilizes after a certain time. Even for 1000 h the mean radius of the grain is below 4 nm for 350 °C annealing, while it is about 2 nm for annealing at 300 °C. When annealing at 400 °C, it can be observed that within 50 h, mean radius of the grain was already above 4 nm, and at around 400 h, it is about 8 nm, while at 1000 h it is 11 nm. During isothermal annealing at 450 °C, within 100 h the mean radius of Al_3Sc grains is about 14 nm and reaches about 30 nm after 1000 h. Notice that even at 1000 h, the mean radius of the grain does not seem to stabilize.

Table 6
Critical findings from Scheil-Gulliver's solidification simulation for 2XXX, 6XXX and 7XXX series of aluminum alloys containing Sc.

Series of Al based alloys	2XXX	6XXX	7XXX
Liquidus temperature (°C)	766.97	799.11	777.27
Temperature (fully Al_3Sc) (°C)	550.433	598.96	603.162
Al_3Sc (mole fraction)	0.02007	0.05966	0.0151
Solid (mole fraction)	0.85692	0.8	0.76797

Fig. 4 shows the nucleation and growth kinetics of Al_3Sc phase during isothermal annealing at 300, 350, 400 and 450 °C for 6XXX alloy, containing high amount of Sc, but no Zr (Sc: 2.60077 wt%). The annealing time simulation was extended to 1000 h to see the effect of time on coarsening of Al_3Sc grains. Here, it can be observed that for isothermal annealing at 300 °C, mean grain size stabilizes at below 4 nm after, which is still twice the mean grain size of that shown for 2XXX alloy with 0.92541 wt% Sc. For isothermal annealing at 350 °C, grain size seems to stabilize, but after 1000 h the mean radius is about 12 nm, that is three times the mean radius of Al_3Sc grains for 2XXX alloy with lower Sc concentration. When annealing at 400 °C, it can be observed that within 100 h, mean radius of the grain is about 16 nm, and at around 400 h, it is about 24 nm. At 1000 h, it is about 34 nm. While for 450 °C, within 100 h, mean radius of Al_3Sc grains is already above 36 nm and reaches about 84 nm after this isothermal annealing for 1000 h. Even at 1000 h, mean radius does not seem to stabilize. In summary, the mean radius of the Al_3Sc grain created during thermal annealing of 6XXX series alloy (that contains a relatively large concentration of Sc) is about 3–4 times as large as the mean radius of Al_3Sc grains for 2XXX series alloy (that contains a relatively low concentration of Sc) isothermally annealed under the same conditions.

As stated before, 2–6 nm mean radius Al_3Sc grains are desired [1], while in some publications even up to 10 nm average grain sizes have been reported [1,6]. Hence, it is important to check the annealing temperature and time prior to performing experiments. The idea behind performing isothermal annealing at a prolonged time (1000 h) at elevated temperatures is that during hot working/ rolling at about 400–600 °C, desired mean radius of Al_3Sc grains is between 20 and 100 nm, as mentioned in the introduction [1]. This was confirmed by the computational results performed for isothermal annealing at 400 °C and 450 °C presented in Fig. 1 and Fig. 2.

4. Conclusions

In this work, we studied the effect of scandium addition in heat treatable aluminum alloys: 2XXX, 6XXX and 7XXX. One candidate alloy was selected from each of these series of alloys after performing phase stability calculations where Sc less than 1 wt% of Sc was added to 2XXX and 7XXX, while more than 1 wt% was added to 6XXX. Alloys 2XXX and 7XXX also contained Zr in addition to Sc, while 6XXX series does not contain Zr. During solidification simulation (Scheil-Gulliver), it was observed that calculated liquidus temperature (melting point) of the

Table 5
Equilibrium amount (mole) of critical phases at a given temperature for 7XXX alloy.

Equilibrium (7XXX)	Temperature	AL3X	Mole fraction of Sc in AL3X	Mole fraction of Al in AL3X	Mole fraction of Zr in AL3X	Mole fraction of Ti in AL3X
	353.4942 °C	0.0202	0.20168	0.75	0.02694	0.02138

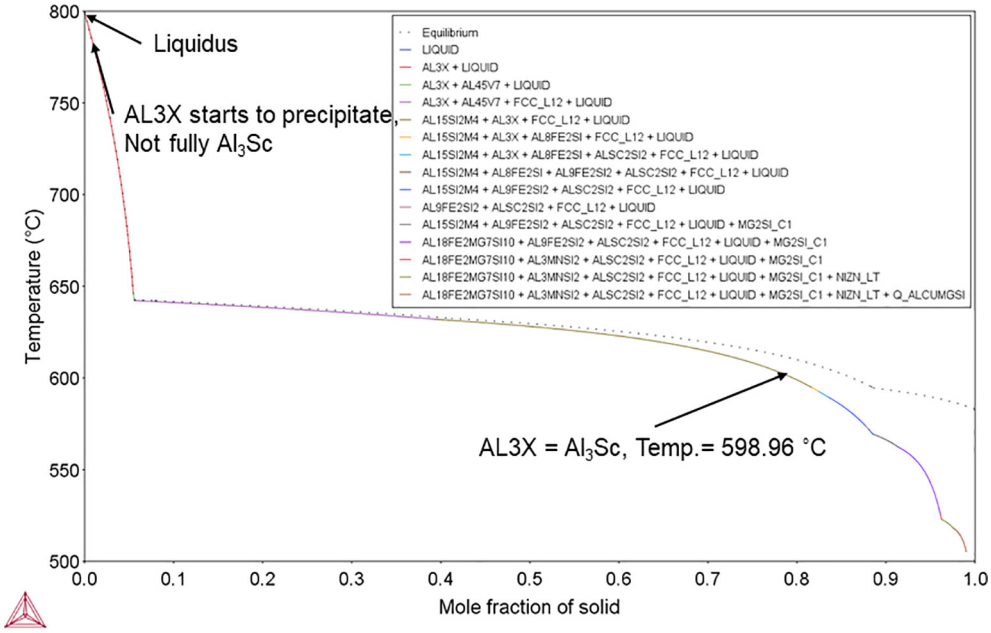

Fig. 1. Scheil-Gulliver solidification simulation results for 6XXX series with Sc.

alloy increases with increase in Sc concentration. These calculations also provided temperatures for initiation of precipitation of various phases as well as the temperature at which AL3X is a fully Al_3Sc phase. Afterwards, heat-treatment simulations were performed for 2XXX and 6XXX alloys at isothermal annealing temperatures of 300, 350, 400 and 450 °C for 1000 h. Results from these calculations demonstrated a significant increase in mean radius of Al_3Sc grains with increase in temperature for both 2XXX and 6XXX alloys. Additionally, a significant increase in the mean radius of Al_3Sc grains for 6XXX alloy containing higher Sc was observed, when compared with 2XXX alloy over the entire duration of annealing. Desired grain sizes for targeted properties of the alloys can be found in the literature. The computational methodology and the results presented in this work can be helpful in determining the composition of the alloy and associated heat treatment. Since scandium is a relatively expensive chemical element which has not been abundantly mined in the past, the focus of this research is on determining the minimum amount of Sc addition that will provide desired microstructural characteristic such as grain size and volumetric concentration. In this work, the focus was on the kinetics only, that is, simulating solidification and nucleation and growth kinetics of precipitation of Al_3Sc phase. This work can be expanded so that it takes into account the equilibrium phases for various compositions and temperatures while using minimum concentration of scandium. Furthermore, this research can be extended to non-isothermal

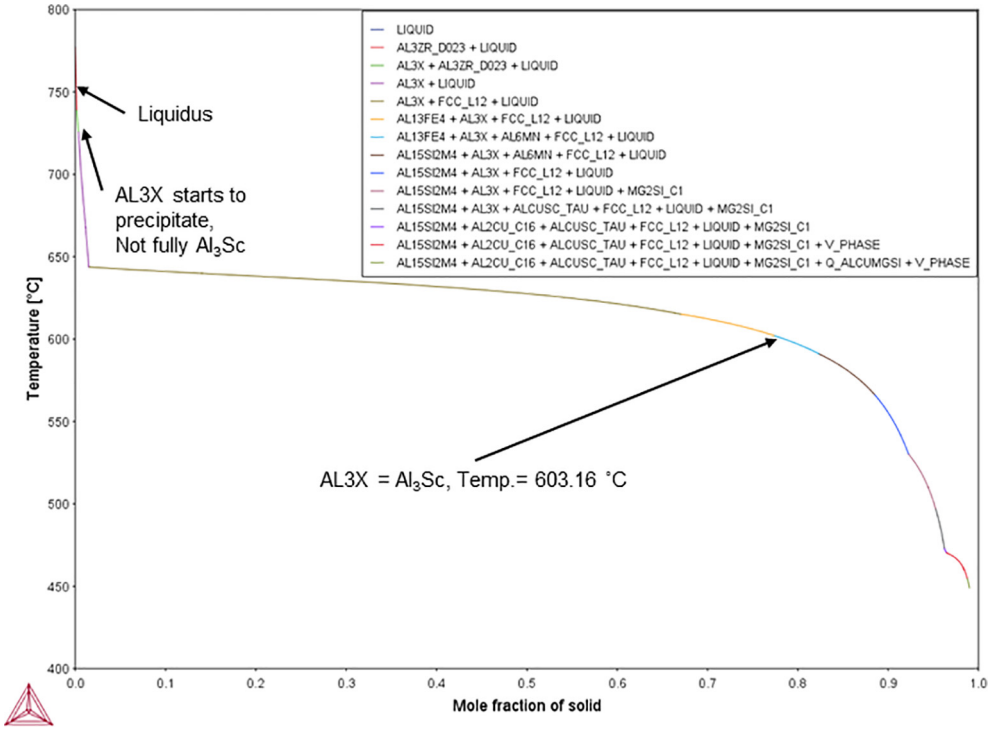

Fig. 2. Scheil-Gulliver solidification simulation results of 7XXX series alloy with Sc and Zr.

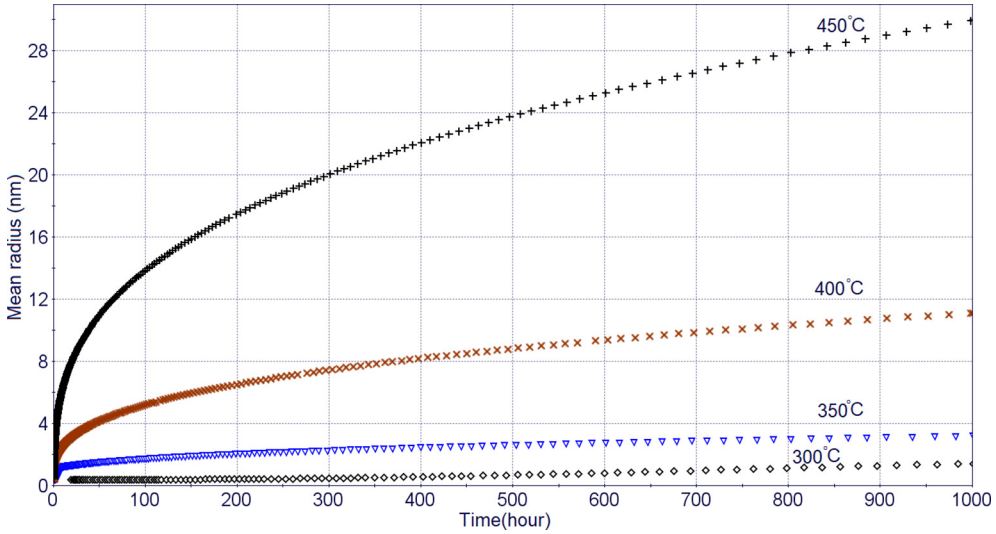

Fig. 3. Al3Sc mean grain radius vs. time at different annealing temperatures for a 2XXX series alloy containing Sc and Zr.

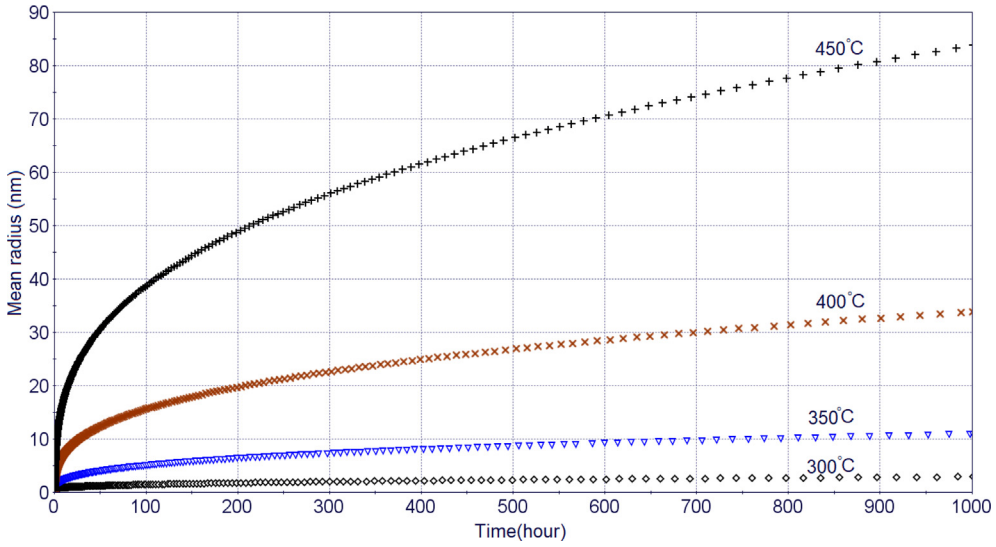

Fig. 4. Al3Sc mean grain radius vs. time at different annealing temperatures for a 6XXX series alloy containing Sc.

annealing so that all the precipitation hardening phases can be simulated simultaneously. Non-isothermal annealing is important as other precipitation hardening phases can only be precipitated at lower temperatures. This finally can lead to optimized non-isothermal annealing protocols.

5. Data availability

This work is part of a ongoing research, so raw data cannot be shared with this article. Regarding interfacial energy, in this work nucleation sites were in the bulk. We are currently working on optimizing interfacial energies at other nucleation sites like dislocations, and grain boundaries. Thus, we have not mentioned our optimized values of interfacial energy in this work. Data will be made available on request. Authors are open to collaboration and can be contacted for setting up model for reproducing the results in case a user encounters a problem.

CRediT authorship contribution statement

Rajesh Jha: Conceptualization, Methodology, Data curation, Writing - original draft, Visualization, Investigation, Writing - review & editing. **George S. Dulikravich:** Conceptualization, Methodology, Supervision, Writing - review & editing.

Declaration of Competing Interest

The authors declare that they have no known competing financial interests or personal relationships that could have appeared to influence the work reported in this paper.

Acknowledgments

Authors would like to express their sincere gratitude to Professor Cristian Ciobanu from Department of Mechanical Engineering, Colorado School of Mines, Golden, Colorado, USA for providing access to some of the commercial software used in this paper. This work was supported by the College of Engineering and Computing at Florida International University and by NASA HQ University Leadership Initiative (ULI) program under federal award number NNX17AJ96A titled “Adaptive Aerostructures for Revolutionary Supersonic Transportation” managed by Texas A&M University.

Appendix A. Supplementary data

Supplementary data to this article can be found online at https://doi.org/10.1016/j.commatsci.2020.109749.

References

[1] J. Røyset, N. Ryum, Scandium in aluminium alloys, Int. Mater. Rev. 50 (1) (2005) 19–44, https://doi.org/10.1179/174328005X14311.

[2] G.N. Haidemenopoulos, A.I. Katsamas, H. Kamoutsi, Thermodynamics-based computational design of Al-Mg-Sc-Zr alloys, Metall. Mater. Trans. A 41A (2010) 888–899.

[3] A. Assadiki, V.A. Esin, M. Bruno, R. Martinez, Stabilizing effect of alloying elements on metastable phases in cast aluminum alloys by CALPHAD calculations, Comput. Mater. Sci. 145 (2018) 1–7, https://doi.org/10.1016/j.commatsci.2017.12.056.

[4] Aluminium alloy: https://en.wikipedia.org/wiki/Aluminium_alloy.

[5] K. Deane, Investigation and modeling of Al3(Sc, Zr) precipitation strengthening in the presence of enhanced supersaturation and within Al-Cu binary alloys, Open Access Dissertation, Michigan Technological University, 2016. http://digitalcommons.mtu.edu/etdr/261.

[6] A.M. Samuel, S.A. Alkahtani, H.W. Doty, F.H. Samuel, Role of Zr and Sc addition in controlling the microstructure and tensile properties of aluminum–copper based alloys, Mater. Des. 88 (2015) 1134–1144.

[7] J.O. Andersson, T. Helander, L. Höglund, P.F. Shi, B. Sundman, Thermo-Calc and DICTRA, computational tools for materials science, Calphad 26 (2002) 273–312.

[8] Thermo-Calc Software: The Precipitation Module (TC-PRISMA) User Guide 2018B (accessed 30 August 2019).

[9] Thermo-Calc Software TCAL5: TCS Aluminium-based Alloys Database v.5 (accessed 30 August 2019).

[10] Thermo-Calc Software MOBAL4: TCS Al-alloys Mobility Database, v4 (accessed 30 August 2019).

[11] C. Zhang, X. Jiang, R. Zhang, X. Wang, H. Yin, X. Qu, Z.K. Liu, High-throughput thermodynamic calculations of phase equilibria in solidified 6016 Al-alloys, Comput. Mater. Sci. 167 (2019) 19–24.

[12] K. Tang, Q. Dua, Y. Li, Modelling microstructure evolution during casting, homogenization and ageing heat treatment of Al-Mg-Si-Cu-Fe-Mn alloys, Calphad 63 (2018) 164–184.

[13] Q. Du, L. Jia, K. Tang, B. Holmedal, Modelling and experimental validation of microstructure evolution during the cooling stage of homogenization heat treatment of Al–Mg–Si alloys, Materialia 4, 70–80, 2018.

[14] P.I. Sarafoglou, A. Serafeim, I.A. Fanikos, J.S. Aristeidakis, G.N. Haidemenopoulos, Modeling of microsegregation and homogenization of 6xxx Al-alloys including precipitation and strengthening during homogenization cooling, Materials 12 (2019) 1421.

[15] P. Priya, D.R. Johnson, M.J.M. Krane, Modeling phase transformation kinetics during homogenization of aluminum alloy 7050, Comput. Mater. Sci. 138 (2017) 277–287.

[16] Q. Du, K. Tang, C.D. Marioara, S.J. Andersen, B. Holmedal, R. Holmestad, Modeling over-ageing in Al-Mg-Si alloys by a multi-phase CALPHAD-coupled Kampmann-Wagner Numerical model, Acta Mater. 122 (2017) 178–186.

[17] J.-G. Jung, Y.-H. Cho, J.-M. Lee, H.-W. Kim, K. Euh, Designing the composition and processing route of aluminum alloys using CALPHAD: case studies, Calphad 64 (2019) 236–247.

[18] Q. Du, W.J. Poole, M.A. Wells, A mathematical model coupled to CALPHAD to predict precipitation kinetics for multicomponent aluminum alloys, Acta Mater. 60 (2012) 3830–3839.

[19] P. Xu, F. Jiang, Z. Tang, N. Yan, J. Jiang, X. Xu, Y. Peng, Coarsening of Al3Sc precipitates in Al-Mg-Sc alloys, J. Alloy. Compd. 781 (2019) 209–215.

[20] R. Jha, G.S. Dulikravich, Determination of composition and temperature regimes for stabilizing metastable precipitation hardening phases in Aluminum alloys with Scandium addition: Combined CALPHAD – Deep Learning Approach (Under Review), 2019.

[21] TensorFlow, https://www.tensorflow.org/.

[22] Keras: The Python Deep Learning library, https://keras.io/.

[23] R. Jha, G.S. Dulikravich, Self-organizing maps to design high temperature Ti-Al-Cr-V alloys for maximum thermodynamic stability, Young's modulus and density, Metals 9 (5) (2019) 537.

[24] R. Jha, F. Pettersson, G.S. Dulikravich, H. Saxen, N. Chakraborti, Evolutionary design of nickel-based superalloys using data-driven genetic algorithms and related strategies, Mater. Manuf. Processes 30 (4) (2015) 488–510.

[25] R. Jha, G.S. Dulikravich, M.J. Colaco, M. Fan, J. Schwartz, C.C. Koch, Magnetic alloys design using multi-objective optimization, Advanced Structured Materials series, Vol. 33, (eds.: A. Oechsner, L.M. da Silva, H. Altenbac.), Properties and Characterization of Modern Materials, pp. 261-284, 978-981-10-1601-1, Springer, Germany, 2017. doi: 10.1007/978-981-10-1602-8_22.

[26] R. Jha, D. Diercks, A. Stebner, C.V. Ciobanu, Metastable Phase Diagram and Precipitation Kinetics of Magnetic Nanocrystals in FINEMET Alloys, https://arxiv.org/abs/1709.08306. (Under Review), 2017.

[27] R. Jha, N. Chakraborti, D. Diercks, A. Stebner, C.V. Ciobanu, Combined machine learning and CALPHAD approach for discovering processing-structure relationships in soft magnetic alloys, Comput. Mater. Sci. 150 (2018) 202–211.

[28] R. Jha, D. Diercks, A. Stebner, C.V. Ciobanu, N. Chakraborti, Interfacial Energy of Copper Clusters in Fe-Si-B-Nb-Cu alloys, Scripta Materialia, (2019) 162, pp. 331–334.

[29] D.R. Diercks, A. Singh, R. Jha, C.V. Ciobanu, A.P. Stebner (2019), A method of nanoscale analysis of the initial stages of crystallization as applied to a FINEMET metallic glass, Materials Characterization, 110026, ISSN 1044-5803, doi: 10.1016/j.matchar.2019.110026.

[30] R. Kampmann, R. Wagner, Decomposition of alloys: The early stages, in: Proc. 2nd Acta-Scripta Metall. Conf., Pergamon, Oxford, 91–103, 1984.

[31] R. Wagner, R. Kampmann, P. W. Voorhees, Homogeneous second-phase precipitation, Materials science and technology, 2001.

[32] Computherm, Precipitation simulation (2017), https://www.nist.gov/sites/default/files/documents/mml/msed/thermodynamics_kinetics/Precipitation-Simulation_CompuTherm.pdf.

[33] J. Langer, K. Schwartz, Kinetics of nucleation in near-critical fluids, Phys. Rev. A 21 (1980) 948.

[34] K.C. Russell, K. Yamauchi, Nucleation in solids: the induction and steady state effects, Adv. Colloid Interface Sci. 13 (1980) 205–318.

[35] W. Kaisheng, S. Gustaf, C. Qing, J. HerngJeng, J. Johan, B. Johan, E. Anders, M. Paul, Simulations of Precipitate Microstructure Evolution during Heat Treatment, 2nd World Congress on Integrated Computational Materials Engineering, Wiley-Blackwell, 201–206, 2013.

[36] J. Agren, Nucleation-a challenge in the modelling of phase transformations, International Conference on Solid-Solid Phase Transformations in Inorganic Materials 2015, PTM 2015, Canada, 9–14, 2015.

[37] M. Bonvalet, T. Philippe, X. Sauvage, D. Blavette, Modeling of precipitation kinetics in multicomponent systems: application to model superalloys, Acta Mater. 100 (2015) 169–177.

[38] Q. Chen, J. Jeppsson, J. Agren, Analytical treatment of diffusion during precipitate growth in multicomponent systems, Acta Mater. 56 (2008) 1890–1896.

[39] S. Li, U.R. Kattner, C.E. Campbell, A computational framework for material design, integrating materials and manufacturing, Innovation 6 (2017) 229–248.

[40] L. Rougier, A. Jacot, C. Gandin, P. Di-Napoli, P. Thery, D. Ponsen, V. Jaquet, Numerical simulation of precipitation in multicomponent Ni-base alloys, Acta Mater. 61 (2013) 6396–6405.

[41] M. Perez, M. Dumont, D. Acevedo-Reyes, Implementation of classical nucleation and growth theories for precipitation, Acta Mater. 56 (2008) 2119–2132.